# Optical model for tubular hollow light guides (1415-RP)

Laouadi, Abdelaziz; Saber, Hamed H.; Galasiu, Anca D.; Arsenault, Chantal



**Publisher's version / Version de l'éditeur:**
https://doi.org/10.1080/10789669.2013.774888
*HVAC and R Research, 19, 3, pp. 324-334, 2013-04-28*

Published in HVAC&R Research (2013), 19(3): 324-334

# Optical model for tubular hollow light guides (1415-RP)

**Abdelaziz Laouadi*, Hamed H. Saber, Anca D. Galasiu, Chantal Arsenault**

*NRC Construction*
*National Research Council of Canada*
*1200 Montreal Road, Ottawa Ontario, K1A 0R6, Canada*
*Tel: (613) 990 6868. Fax: (613) 954 3733*
* *Corresponding author. Email: aziz.laouadi@nrc-cnrc.gc.ca*

## Abstract

*Tubular hollow light guides are found in many lighting and daylighting systems to transport collected light into deep spaces of building interiors. Linear straight guides are popularly used due to their high optical efficiency, but non-linear guides with bended sections are sometimes required to fulfill some installation restrictions. The optical performance of such bended guides is, however, unknown. This paper presents the development, validation and application of an optical model to compute the transmittance of light guides with and without bends. The model is based on the ray-tracing technique, and can handle segmented guides with connection elbows. Measurement of the light transmittance of a light guide with two connection elbows is conducted using an outdoor large integrating box to benchmark the model. The model predictions are in good agreement with the measurement and public data for vertical light guides without bends. The model predictions for bended light guides installed in a northern mid-latitude location show that orienting the middle pipe section of the guide towards the north direction results in better control of sunlight and solar heat gains than other orientations.*

## Introduction

Hollow light guides are found in many daylighting and electrical lighting systems such as tubular daylighting devices, core sunlighting systems, and warehouse and tunnel electrical lighting systems (Laouadi and Coffey, 2012; Aizenberg, 2010; Kim and Kim, 2010; Hien and Chirarattananon, 2009; Kwok and Chung, 2008; CIE, 2006; CIE, 2005). Hollow daylight guide systems consist of tubular or rectangular pipes to transport the collected light from the building facades and roofs into deep spaces of building interiors. The interior surface of the guide is lined with highly specularly reflective coatings, or prismatic optical elements to maintain a high optical efficiency of long guides. Linear straight guides are popularly used in buildings, but non-linear guides with a number of bended sections are sometimes required to fulfill some installation restrictions. The optical performance of such bended guides is, however, unknown.

Theoretical investigations of the guide's optical performance have been mainly limited to the linear straight guides without bends. Zastrow and Wittwer (1986) and Nutter et al. (1988) were among the first researchers to develop an analytical model for the light transmittance of tubular guides. Swift and Smith (1995) used a ray tracing method to develop an enhanced transmittance model. Swift and Smith (2008) extended their previous work to include rectangular straight guides. Swift (2010) developed a model for light transmittance of splayed rectangular guides, and Edmonds (2010) followed up with expressions for the calculation of the beam and diffuse transmittance of tubular straight guides with rectangular, triangular, rhombic and hexagonal cross-sections.

Computer simulations have also been used to predict the guide's light transmittance. Laouadi and Arsenault (2003) developed the SkyVision computer program (NRC, 2011) to address the optical performance of linear guides of tubular daylighting devices. Kocifaj et al. (2008) developed the HOLIGILM computer program to address the distribution of indoor illuminances in a rectangular room from vertical tubular guides under direct sunbeam and sky diffuse light. Subsequent work by the authors (Kocifaj et al., 2010) extended the software capabilities to include guides with bends (connection elbows are the intersection geometry domains of two relatively tilted pipe segments). Chirarattananon et al. (2010) and Samuhattananon et al. (2011) developed complex algorithms using the ray-tracing technique to compute the light transmittance of tubular guides with and without bends (connection elbows are simulated as torus sections with an interior radius equal to the guide's radius).

## Objectives

This paper is a part of the ASHRAE research project 1415-RP: Thermal and lighting performance of tubular daylighting devices (TDD's). The aim of the project is to develop detailed and validated algorithms to compute the thermal and lighting performance metrics of TDD's. The specific objectives of this paper are:

- To develop an analytical model to compute the optical characteristics (transmittance, and absorptance) of linear and non-linear light guides;
- To validate the optical model, by comparing its predictions for transmittance with the measurements and literature data; and
- To explore the effect of bended light guides on their optical performance.

## Mathematical formulation

Figure 1 shows a schematic representation of a typical non-linear tubular guide with connection elbows. The guide is characterized by its internal radius ($R_p$), and may have three different sections: upper, middle and lower sections with respective lengths ($L_{pu,}$ $L_{pm}$, $L_{pl}$ ). The upper section may be tilted with an angle of ($\pi/2 - \lambda_c$) from the horizontal, and its revolution axis may be oriented towards a given direction with an azimuth angle ($\psi_c$) from the south direction. The middle section is connected with the upper section with an elbow of an angle ($\lambda_{pu}$), and may be oriented towards a different direction with an azimuth angle ($\psi_{pm}$) from the south direction. The lower section is vertical, and is joined with the middle section using an elbow with an angle ($\lambda_{pl} = \lambda_{pu} + \lambda_c$; with $\lambda_{pl} \leq \pi/2$).

## ASSUMPTIONS

The following assumptions are made for the model development:

- The guide is circular, and its interior lining is opaque and specular (mirror-like); and
- The incident luminous flux is uniformly distributed over and absorbed by the pipe surfaces.

Before proceeding to the model development, three coordinates systems are defined. First, an absolute fixed coordinate system ($x_0$, $y_0$, $z_0$) is considered having the x-axis facing the south direction, y-axis facing the east

direction, and z-axis parallel to the vertical. The inclination and orientation angles ($\lambda$, $\psi$) of the guide sections are defined in this system. The angular coordinates of a given point (p) are noted as ($\theta$ from the $z_0$-axis; $\psi$ from the $x_0$-axis, positive counter-clockwise) in this system. Second, an additional fixed reference system ($x_{ref}$, $y_{ref}$, $z_{ref}$) is defined in the entrance plane of the upper pipe section. The reference x-axis (oriented opposite to the entrance plane direction) makes an azimuth angle $\psi_{ref}$ from the south direction and is tilted from the horizontal at an angle $\lambda_c$. The absolute angular coordinates of a point p($\theta$, $\psi$) are transformed to their equivalent angles ($\Theta$ from $z_{ref}$-axis; $\Psi$ from $x_{ref}$-axis, positive counter-clockwise) in the reference system. A third mobile system (x, y, z) is defined in the entrance plane of each pipe section with the z-axis is parallel to the revolution axis of the pipe section. The x-axis and y-axis of the mobile system of the upper pipe section are rotated around the revolution z-axis to track the sun movement in the sky so that the y-axis is in the same vertical plane of the incident sunbeam rays. In the following, calculations will be performed in the mobile coordinate system. Laouadi et al. (2012a) presented a method for the coordinate transformation from one system to another.

Consider a conical beam ray emanating from a point whose coordinates are defined in the mobile system p($x_{p,pu}$, $y_{p,pu}$, $z_{p,pu}$). The conical ray reaches the entrance plane of the upper pipe section at directional angles ($\Theta_{pu}$ from the z-axis, $\Psi_{pu}$ from the reference x-axis). The incident ray will undergo multiple repetitive reflections at the inner pipe surface until it reaches the pipe's exit plane. Figure 2 shows the projected path of the conical beam ray onto the entrance plane of the upper pipe section. The length (period) of the repetitive reflections for each pipe section is given by the following relations:

(1)

(2)

(3)

where:

$d_{pu}$ : distance between two consecutive ray's reflections projected onto the entrance plane of the upper pipe (m, ft);

$d_{pm}$ : distance between two consecutive ray's reflections projected onto the entrance plane of the middle pipe (m, ft);

$d_{pl}$ : distance between two consecutive ray's reflections projected onto the entrance plane of the lower pipe (m, ft);

$L_{r,pu}$ : distance between two consecutive ray's reflections along the length of the upper pipe (m, ft);

$L_{r,pm}$ : distance between two consecutive ray's reflections along the length of the middle pipe (m, ft);
$L_{r,pl}$ : distance between two consecutive ray's reflections along the length of the lower pipe (m, ft);
$\Theta_{pu}$ : angle between the incident ray direction and the revolution z-axis of the upper pipe (radians);
$\Theta_{pm}$ : angle between the incident ray direction and the revolution z-axis of the middle pipe (radians);
$\Theta_{pl}$ : angle between the incident ray direction and the revolution z-axis of the lower pipe (radians).

Assuming that the pipe inner surface is specular, that is, it reflects incident rays in the mirror direction, the projected distance $d_{pu}$ for the upper pipe is expressed as follows:

(4)

where $\mu_{pu}$ is the reflection angle projected onto the upper pipe's entrance plane. Similar relationships may be developed for the other pipe sections. The reflection angle ($\mu_{pu}$) is given by the following relation:

(5)

where:
$\varphi''_{p,pu}$ : relative azimuth angle of the incident ray emanating from the point (p) with respect to the x-axis (radians);
$\varphi'_{1,pu}$ : relative azimuth angle of the first ray's reflection point with respect to the x-axis (radians).

The angle $\varphi''_{p,pu}$ may be expressed as a function of the ray's directional angle $\Psi_{pu}$ as follows:

(6)

where $\Psi_{x,pu}$ (transformed of $\psi_{x,pu}$) is the relative azimuth angle of the x-axis associated with the upper pipe with respect to the direction of the reference x-axis, given by the following relation:

$$\Psi_{x,pu} = \begin{cases} \cos^{-1}\left(\frac{\cos}{\sqrt{1-\sin}}\right. \\ \psi_{x,pu} - \psi_1 \end{cases} \quad (7)$$

with:

(8)

(9)

where:

$\lambda_c$ : tilt angle from the horizontal of the entrance plane of the upper pipe section (radians);
$\psi_c$ : azimuth angle of the upper pipe section with respect to the south direction (radians);
$\psi_{ref}$ : azimuth angle of the reference x-axis with respect to the south direction (radians);

$\psi_{sun}$ : solar azimuth angle with respect to the south direction (positive counter clockwise) (radians);

$\psi_{x,pu}$ : azimuth angle of the mobile x-axis attached to the upper pipe section with respect to the south direction (radians);

By considering that the first ray's reflection point and the point (p) are in the same projected line, one obtains:

$$\varphi'_{1,pu} = \pi + \varphi''_{p,pu} - \sin^{-1}(\quad \tag{10}$$

Note that Equation (10) admits a real solution if the conical ray emanating from the point (p) intersects with the entrance plane of the upper pipe.

The number of reflections that a ray undergoes at the inner surface of the upper pipe is given by the following relationship:

$$N_{pu} \tag{11}$$

where $L_{0,pu}$ is the distance along the pipe's revolution z-axis from the pipe's entrance plane to the first ray's contact point with the pipe surface. By referring to Figure 2, the distance $L_{0,pu}$ may be obtained as follows:

(12)

where $d_{0,pu}$ is the projected distance as shown in Figure 2, given by:

$$d_{0,pu} = \quad \tag{13}$$

The conical ray exits the upper pipe at the last reflection point whose relative azimuth angle ($\varphi'_{N,pu}$) with respect to the direction of the mobile x-axis is given by:

$$\varphi'_{N,pu} = \begin{cases} \varphi'_{p,pu}, & \text{if } N_{pu} = \\ (2N_{pu} - 1) \cdot \varphi'_{1,} \end{cases} \tag{14}$$

The relative azimuth angle ($\varphi''_{N,pu}$) from the x-axis of the last reflected ray (after undergoing N reflections) exiting the pipe section is given by the following relation:

$$\varphi''_{N,} \tag{15}$$

The previous analysis can also be applied to the middle and lower pipe sections with a proper transformation of the system of coordinates. For the middle pipe section, the mobile system of coordinates (x, y, z) of the upper pipe section is rotated around the z-axis with an angle ($\Delta\Psi$), and then counter-clockwise around the x-axis with an angle

equal to $\lambda_{pu}$, and then translated along the y-axis and z-axis to account for the elbow curvature so that the new system of coordinates is centered in the plane of the entrance surface of the middle pipe with the new z-axis parallel to its revolution axis (Figure 2). The relative azimuth angle ($\Delta\Psi$) is expressed as follows:

(16)

where $\Psi_{x,pm}$ (transformed of $\psi_{x,pm}$) is the relative azimuth angle from the reference x-axis of the projected x-axis associated with the middle pipe onto the plane of the upper pipe's entrance surface. Equation (7) is used to convert the azimuth angle ($\psi_{x,pm}$) of the x-axis of the middle pipe section with respect to the south direction to its relative azimuth angle ($\Psi_{x,pm}$) with respect to reference x-axis. The azimuth angle ($\psi_{x,pm}$) is expressed as a function of the azimuth angle of the middle pipe ($\psi_{pm}$) as follows:

(17)

The last ray's reflection point off the upper pipe surface will have the following coordinates expressed in the coordinate system attached to the upper pipe section:

(18)

(19)

(20)

To repeat the same scenario of the ray's reflections in the middle pipe section, the coordinates ($x_{e,pu}$, $y_{e,pu}$, $z_{e,pu}$) of the intersection point of the last reflected ray with the exit plane of the upper pipe section is determined using suitable relationships of line intersection with a plane. The coordinates of the ray exit point p($x_{e,pu}$, $y_{e,pu}$, $z_{e,pu}$) will then have to be transformed to the coordinate system attached to the middle pipe section to become the entrance point p($x_{p,pm}$, $y_{p,pm}$, $z_{p,pm}$) of the incident rays on the elbow surface between the upper and middle pipe sections. The coordinate transformations (see details in Laouadi et al., 2012a) are expressed by the following relations:

$$\begin{bmatrix} x_{p,pm} \\ y_{p,pm} - y_{cc,pm} \\ z_{p,pm} - z_{cc,pm} \end{bmatrix} = \begin{bmatrix} 1 & 0 & \\ 0 & \cos\lambda_{pu} & s \\ 0 & -\sin\lambda_{pu} & c \end{bmatrix} \tag{21}$$

with:

(22)

The poplar and relative azimuth angles ($\Theta_{pm}$, $\varphi''_{p,pm}$) of the last reflected ray off the upper pipe section expressed in the coordinate system associated with the middle pipe is obtained using the coordinate transformation from the upper to the middle pipe sections. Equations (135) to (137) in the Appendix of Laouadi et al. (2012a) are used by substituting the following variables:

$$\Theta_{pm} \leftarrow \Theta_p; \quad \varphi''_{p,pm} \leftarrow \Psi_p + \frac{\pi}{2}; \quad \theta_p = \Theta_{pu}; \quad \lambda_c = \lambda_{pu}; \quad \psi_p = \varphi''_{N,pu} \tag{23}$$

The relative azimuth angle ($\varphi'_{p,pm,}$) of the ray's entrance point to the elbow surface between the upper and middle pipe sections, expressed in the coordinate system associated with the middle pipe section, is derived from the point coordinates as follows:

(24)

Rays exiting from the upper pipe section may undergo several reflections off the elbow surface before entering the middle pipe section or reflecting backwards to the upper pipe section. The algorithm in the Appendix is used to compute the coordinates of the intersection point of the incident rays with the elbow exit plane (or entrance plane of the middle pipe), and the directional angles of the exiting rays from the elbow exit plane. Those coordinates are treated as inputs to the middle pipe section. Equations (4) to (15) are, thus, applied to the middle pipe section to calculate the number of reflections ($N_{pm}$), and the directional angles of exiting rays ($\varphi'_{N,pm}$, $\varphi''_{N,pm}$) from the middle pipe.

For the lower pipe section, the system of coordinates (x, y, z) associated with the middle pipe section is rotated around its x-axis with an angle equal to $-\lambda_{pl}$ (as in Figure 2), and then translated along the y-axis and then the z-axis so that the new coordinate system is centered in the plane of the entrance surface of the lower pipe and the z-axis is

parallel to its revolution axis . The last ray's reflection point at the middle pipe surface will have the following coordinates expressed in the coordinate system attached to the middle pipe section:

(25)

(26)

$$\mathbf{z}_{\mathbf{i}} \tag{27}$$

To repeat the same scenario of the ray's reflections in the lower pipe section, the coordinates ($x_{e,pm}$, $y_{e,pm}$, $z_{e,pm}$) of the intersection point of the last reflected ray with the exit plane of the middle pipe section is determined using suitable relationships of line intersection with a plane. The coordinates of the ray exit point p($x_{e,pm}$, $y_{e,pm}$, $z_{e,pm}$) will then have to be transformed to the coordinate system attached to the lower pipe section to become the entrance point p($x_{p,pl}$, $y_{p,pl}$, $z_{p,pl}$) of the incident rays on the elbow surface between the middle and lower pipe sections. The coordinate transformations (see details in Laouadi et al., 2012a) are expressed by the following relations:

(28)

with:

(29)

The poplar and relative azimuth angles ($\Theta_{pl}$, $\varphi"_{p,pl}$) of the last reflected ray off the middle pipe section expressed in the coordinate system associated with the lower pipe is obtained using the coordinate transformation from the middle to the lower pipe sections. Equations (140) to (142) in the Appendix of Laouadi et al. (2012a) are used by substituting the following variables:

$$\Theta_{pl} \leftarrow \Theta_p;\ \varphi''_{p,pl} \leftarrow \psi_p + \frac{\pi}{2};\quad \Theta_p = \Theta_{pm};\ \lambda_e = \lambda_{pl}; \tag{30}$$

The relative azimuth angle ($\varphi'_{p,pl,}$) of the ray's entrance point to the elbow surface between the middle and lower pipe sections, expressed in the coordinate system associated with the lower pipe section, is derived from the point coordinates as follows:

(31)

Rays exiting from the middle pipe section may undergo several reflections off the elbow surface before entering the lower pipe section or reflecting backwards to the middle pipe section. The algorithm in the Appendix is again used to compute the coordinates of the intersection point of the incident rays with the elbow exit plane (or entrance plane of the lower pipe), and the directional angles of the exiting rays from the elbow exit plane. Those coordinates are treated as inputs to the lower pipe section. Equations (4) to (15) are, thus, applied to the lower pipe section to calculate the number of reflections ($N_{pl}$), and the directional angles of the exiting rays ($\varphi'_{N,pl}$, $\varphi''_{N,pl}$). Since the lower pipe is horizontal, the polar angle ($\theta_{pl}$) from the vertical and the azimuth angle ($\psi_{pl}$) from the south direction of rays exiting from the lower pipe are given by the following equation:

(32)

## BEAM OPTICAL CHARACTERISTICS

To evaluate the optical characteristics (transmittance, and absorptance) of the tubular guide, the incident rays are assumed collimated (parallel) and fully covering the entrance surface of the upper pipe section. The points where the incident rays emanate from are thus situated on the entrance surface of the upper pipe ($z_{p,pu} = 0$). The relative azimuth angle of the incident rays are set equal to $\varphi''_{p,pu} = \pi/2$. The forgoing analysis, equations (1) to (32), may be used to evaluate the transmitted and absorbed luminous fluxes of the guide. The portion of the luminous flux carried out by the conical ray at the lower pipe exit surface, and the portion absorbed by the inner surfaces of the guide sections are expressed as follows:

$$\tau_{pp}(\theta_{pu}, \Psi_{pu}) = \rho_{pu}^{N_{pu}}(\theta_{pu}) \cdot \rho_{epu}^{N_{epu}}(\theta_{pu}) \cdot \rho_{p}^{N} \tag{33}$$

(34)

where:

$N_{epu}$ : number of ray's reflections at the upper elbow surface;

$N_{epl}$ : number of ray's reflections at the lower elbow surface;

$\alpha_{pp}$ : absorptance of the tubular guide for a conical beam ray incident on the pipe entrance surface at directional angles $\Theta_{pu}$ and $\Psi_{pu}$;

$\rho_{epu}$ : reflectance of the interior surface of the upper elbow for a conical beam ray incident at an angle $\Theta_{pu}$ on the entrance surface of the upper pipe;

$\rho_{epl}$ : reflectance of the interior surface of the lower elbow for a conical beam ray incident at an angle $\Theta_{pm}$ on the entrance surface of the middle pipe;

$\rho_{pu}$ : reflectance of the interior surface of the upper pipe for a conical beam ray incident at an angle $\Theta_{pu}$ on the entrance surface of the upper pipe;

$\rho_{pm}$ : reflectance of the interior surface of the middle pipe for a conical beam ray incident at an angle $\Theta_{pm}$ on the entrance surface of the middle pipe;

$\rho_{pl}$ : reflectance of the interior surface of the lower pipe for a conical beam ray incident at an angle $\Theta_{pl}$ on the entrance surface of the lower pipe;

$\tau_{pp}$ : transmittance of the tubular guide for a conical beam ray incident on the pipe entrance surface at directional angles $\Theta_{pu}$ and $\Psi_{pu}$.

Equation (34) stipulates that the backward reflected rays (if any) exiting from the pipe entrance surface, are negligible. The total transmittance ($\tau_{pipe}$) and absorptance ($\alpha_{pipe}$) of the tubular guide for collimated (parallel) rays incident on the pipe entrance surface are obtained by integration of Equations (33) and (34) over the pipe entrance surface as follows:

(35)

(36)

The integral in Equation (35) may be evaluated using a suitable numerical integration method such as the Gauss quadrature or Simpson's method.

## DIFFUSE OPTICAL CHARACTERISTICS

The diffuse optical characteristics ($\tau_{d,pipe}$, $\alpha_{d,pipe}$) of the tubular guide are obtained by integrating Equations (35) and (36) over a hemisphere with a uniform luminance:

(37)

(38)

## Model Benchmarking

The model predictions for the guide transmittance are benchmarked with new measurement results, and currently-available public data.

Public transmittance data exist mainly for vertical light guides without bends, and those for the bended guides (Kocifaj et al., 2010; Chirarattananon et al., 2010; Samuhattananon et al., 2011) used different shapes for the connection elbows, and, therefore, cannot directly be compared with the present model. Figure 3 presents the inter-model comparison for vertical light guides with a pipe reflectance of 95% and various aspect ratios (length over diameter, L/D). The predictions from the present model compare very well with the other models.

For the experimental model benchmarking, an outdoor large integrating cubic box of 2 m (76.5") height was built and calibrated to measure the visible transmittance of tubular daylighting devices (TDD's) under direct sunlight. Two commercially available and one custom-made TDD's were tested to validate a newly-developed optical model for TDD's (Laouadi et al., 2012a). The custom-made TDD had a pipe with three sections joined by two discrete elbows (intersection geometry domain of two relatively tilted pipes). The pipe entrance plane was covered by a 3 mm (1/8") clear polycarbonate sheet, and the exit plane was covered by a double glazed commercial diffuser. The interior surface of the pipe was coated with an enhanced silver film with a visible reflectance of 98% at a normal incidence angle. The angular profile of the visible transmittance of the diffuser was measured on-site using the integrating box. Figure 4 shows the geometrical details of the custom-made TDD.

The light transmittance of the custom-made TDD was measured for three pipe orientations (the middle pipe section faced the south, north, and west direction; the upper and lower pipe sections were vertical). The measurement was conducted under sunny days in the summer and fall 2011 at Ottawa (latitude = 45.32$^{o}$ north, and longitude = 75.67$^{o}$ east), Ontario, Canada. The estimated uncertainty of the measurement procedure was 10%. More details on the measurement procedure and validation study of the TDD optical model may be found in Laouadi et al. (2012b). Figure 5 shows a typical comparison between the measured and predicted visible transmittance for the custom-made TDD when the middle pipe section was oriented towards the west direction. Given the uncertainty of the measurement procedure (10%), the model predictions are in good agreement with the measurements, within an average deviation of 14% (from 8:00 to 16:00), and a maximum deviation of 24%. The maximum deviation occurred in the morning (around 9:30) and afternoon hours (around 14:00) when the sun was directly facing the elbow surface. This large deviation could be attributed to the effect of the shape of the elbow

section. The discrete elbow section of the custom-made TDD was made by joining the pipe sections together (see Figure 4). The present model, however, uses a smooth elbow section, section of a "horn" torus (see Figure 1, and the red dotted line in Figure 4). Smooth elbow surfaces redirect better the incident rays than discrete elbow surfaces, and, therefore, result in higher transmittance.

### Optical performance of bended light guides

The presence of elbows in light guides can significantly affect their optical performance. A good practice should optimize the guide light transmission efficiency by a proper orientation of the guide sections during the guide installation process at a given location. Figure 6 shows the angular profile of transmittance of guides with two elbows and various orientation angles of the middle pipe section (the upper and lower pipe sections are vertical) when sunbeam light is due south. The guide has the following dimensions: $R_p$ = 178 mm (7"), $L_{pu} = L_{pl}$ = 300 mm (1 ft), and $L_{pm}$ = 900 mm (3 ft), with an aspect ratio L/D ≈ 4.3. The pipe reflectance is fixed to 98%. Vertical guides without bends are more efficient than bended guides for low incidence angles (< 60°; e.g., noon summer times), and less efficient for higher incidence angles (> 60°; e.g., noon winter times). Bended guides facing the north direction result in the lowest transmittance for low incidence angles (< 35°) and highest transmittance for higher incidence angles. Guides facing the south direction result in reversed trends to the north direction. Light guides oriented towards the east or west direction provide average results between the north and south orientations.

In view of the results of Figure 6, the optical performance of bended light guides depends on the geographical location where they are installed, and the time of the day and year. Figures 7 to 9 show the hourly profiles of transmittance of light guides installed in Ottawa, Ontario, Canada for three typical days in summer, fall and winter, respectively. Vertical light guides without bends outperform bended light guides, except at early mornings or late afternoons in winter. Orienting guides towards the north direction result in better control of sunlight and solar heat gains as they reduce the transmittance in summer times when there is abundance of the outdoor daylight, and increase the transmittance in the shoulder seasons when there is not enough outdoor daylight.

It should be noted that the results of Figures 7 to 9 apply only to the guide geometry and installation location as specified above. Light guides with other geometries installed in different locations may result in different optical performance. The developed optical model may, thus, aid in the design of an optimized installation of bended guides for a specific installation location.

## Conclusion

This paper presented the development, validation and application of an optical model to compute the transmittance of straight and bended tubular hollow light guides. The model was based on the ray-tracing technique, and can handle segmented guides with connection elbows. The model was benchmarked with new measurement of the light transmittance of bended guides, and public transmittance data for vertical guides without bends.

An outdoor large integrating box was built and calibrated to measure the light transmittance of a custom-made light guide under direct sunlight to benchmark the developed model. The integrating box procedure was benchmarked by comparing its measurement with the manufacturer data of a clear polycarbonate sheet. The results compared within a 5% deviation, lower than the estimated uncertainty of the measurement (10%). The custom-made guide had three pipe segments with two connection elbows. The guide's entrance plane was covered by the clear polycarbonate sheet, and the exit plane was covered by a double glazed commercial diffuser. The light transmittance of the custom-made guide was measured under sunny days in the summer and fall 2011 at Ottawa, Ontario, Canada, for three pipe orientations (the middle pipe segment faced the south, north, and west direction; the upper and lower pipe segments were vertical). The model predictions were in good agreement with the measurements, within an average deviation of 14%, and a maximum deviation of 24% (occurred when the sun was directly facing the elbow surface). This large deviation could be attributed to the effect of the shape of the elbow section. The discrete elbow section of the custom-made guide was made by joining the pipe segments together whereas the present model used a smooth elbow section (section of a "horn" torus). Smooth elbow surfaces redirect incident sunlight better than discrete elbow surfaces, and, therefore, result in higher transmittance. Furthermore, the model predictions for vertical guides without bends compared very well with the public light transmittance data.

The optical model was applied to bended guides installed in a northern mid-latitude location (Ottawa, Ontario, Canada) to show the effect of the guide bends on the guide's optical performance. The tested guide had three pipe segments and two connection elbows with an aspect ratio $L/D \approx 4.3$. The upper and lower pipe segments were vertical and the middle pipe segment could be tilted and oriented to face a particular direction. The results showed that the optical performance of bended light guides depends on the geographical location where they are installed, and the time of the day and year. For the northern location under consideration, vertical light guides without bends were found to outperform bended light guides, except at early mornings or late afternoons in winter. To better

control sunlight and undesired solar heat gains in summer, bended light guides should be oriented towards the north direction as they reduce the transmittance in the summer times when there is abundance of the outdoor daylight, and increase it in the shoulder seasons when there is not enough outdoor daylight. One should, however, be careful to generalize the obtained results as the optical performance of bended light guides depends on their geometrical dimensions (diameter and length of pipe sections) and the geographical location where they are installed. The developed model may, therefore, assist in the design of optimized bended light guides to efficiently use sunlight throughout a year in a particular installation site.

**Acknowledgement**

This work was jointly funded by ASHRAE under the Research Project 1415-RP, and the Construction Portfolio of the National Research Council of Canada. The authors were very thankful for their financial support. The authors would also like to thank Solatube International Inc., VELUX America Inc., and ODL Inc. for their in-kind support to the project.

## Nomenclature

$d$ : distance between two consecutive ray's reflections projected onto the entrance plane of a pipe section (m, ft);

$d_0$ : projected distance onto the pipe entrance plane of the ray's path between its incidence point and first contact point with the pipe surface (m, ft)

$L$ : length (m, ft)

$L_0$ : distance along the pipe's revolution z-axis from the pipe's entrance plane to the first ray's contact point with the pipe surface (m, ft)

$N$ : number of ray's reflections off a surface;

$R_p$ : internal radius of the pipe cross-section (m, ft)

$x$ : x-coordinate of a point (m, ft)

$y$ : y-coordinate of a point (m, ft)

$z$ : z-coordinate of a point (m, ft)

**Greek symbols**

$\alpha$ : absorptance

$\alpha_{pp}$ : absorptance of the tubular guide for a conical beam ray incident on the guide's entrance surface

$\alpha_{pipe}$ : absorptance of the tubular guide for collimated beam rays incident on the guide's entrance surface

$\lambda$ : slope angle of a surface from the horizontal (radians)

$\varphi'$ : relative azimuth angle of the ray's reflection point from the x-axis attached to a guide section (radians).

$\varphi''$ : relative azimuth angle of the incident ray from the x-axis attached to a guide section (radians)

$\varphi''_N$ : relative azimuth of the last reflected ray from the x-axis attached to a guide section (radians)

$\mu$ : reflection angle between the incident and reflected ray's path projected onto the entrance plane of a guide section

$\theta$ : polar angle from the z-axis of a reference coordinate system (radians)

$\rho$ : reflectance

$\tau$ : transmittance

$\tau_{pp}$ : transmittance of the tubular guide for a conical beam ray incident on the guide's entrance surface

$\tau_{pipe}$ : transmittance of the tubular guide for collimated beam rays incident on the guide's entrance surface

$\lambda$ : slope angle of a surface from the horizontal (radians)

$\Psi$ : azimuth angle from the reference x-axis (radians)

$\Psi_x$ : azimuth angle of the mobile x-axis from the reference x-axis (radians)

$\psi$ : azimuth angle from the south direction (radians)

$\psi_{pm}$ : azimuth angle of the revolution z-axis of the middle guide section from the south direction (radians)

$\psi_x$ : azimuth angle of the mobile x-axis from the south direction (radians)

**Subscripts**

c : guide's entrance plane

epu : upper elbow

epl : lower elbow

p : point

pu : upper guide section

pm : middle guide section

pl : lower guide section

## Appendix – Algorithm for ray reflection at an elbow surface

The following computational algorithm is used to trace ray's reflections at an elbow surface from its entrance point to its exit point from the elbow. Figure 10 shows a schematic description of a ray's reflection path at an elbow surface.

Tubular light guides may include two types of elbows with discrete and smooth surfaces. A discrete elbow is the intersection geometry domain between the upper and lower pipes. A smooth elbow is a section of a torus surface. A torus section is characterized by its interior and exterior radii. In this paper, a smooth elbow surface with a zero interior radius is considered (such as shown in Figure 10), but the following algorithm may be applied to any elbow type.

Two coordinates systems are defined for an elbow surface, which are attached to the upper and lower pipe sections as shown in Figure 10. The following algorithm is used to compute the coordinates of the ray's exit point ($P_3$) from the elbow exit plane:

1. In the coordinates system attached to the pipe section above the elbow entrance plane, compute the coordinates of the intersection point $P_1$ with the elbow entrance plane of a ray reflecting off the pipe surface at point $P_0$ (with given coordinates) using relationships of a line intersection with a plane.
2. Transform the coordinates of $P_1$ to the coordinate system attached to the pipe section below the elbow exit plane using Equation (21) or (28).
3. For a ray emanating from the point $P_1$, compute the coordinates of the ray's intersection point $P_3$ with the elbow exit plane (see the dashed line in Figure 10), and check if the point is within the surface of the exit plane if its radius to the centre of the plane is lower than the pipe radius, otherwise the ray will intersect with the elbow surface at $P_2$.
4. If the ray intersects with the elbow surface, compute the coordinates of the intersection point $P_2$ using relationships of a line intersection with a torus surface of equation:

$$F = x^2 \tag{39}$$

where $R_p$ is the pipe radius, and $\delta = -1$ or $+1$ for the upper or lower pipe elbow (see Figure 1), respectively. Note that Equation (42) is written in the coordinate system attached to the pipe section below the elbow.

5. At point $P_2$, calculate the directional angles ($\Theta_r$ from the z-axis, $\varphi"_r$ from the x-axis) of the reflected ray based on the directional angles of the surface inward normal ($\lambda_n$ from the z-axis; $\varphi'_n$ from the x-axis) at $P_2$ and the directional angles ($\Theta_i$, $\varphi"_i$) of the incident ray from $P_1$ using the law of reflection (see more details in Laouadi et al., 2012c). The surface inward normal vector at $P_2$ may be obtained by calculating the gradient of the elbow function ($-\nabla F$). The directional angles of the inward normal vector may be given by:

$$\cos\lambda_n = -\frac{\partial F}{\partial z} / |\nabla F|; \tag{40}$$

Note that if $\lambda_n$ is negative (surface is facing downwards), use the complementary angle $\lambda_n = \pi + \lambda_n$.

6. Compute the intersection points of the reflected ray at $P_2$ with the elbow entrance and exit planes. If the reflected ray does not intersect with the elbow entrance and exit planes, it will intersect with the elbow surface.
7. If the reflected ray at $P_2$ intersects again with the elbow surface, steps 4 to 6 are repeated until the reflected ray intersects with elbow entrance or exit plane.
8. Compute the number of reflections ($N_{elbow}$) of the incident ray from $P_1$ onto the elbow surface.

## References


Aizenberg, J. B. 2010. Outcome of research, developments, production and application of extended hollow light guides (1964-2009). Proceedings of the CIE 2010"Lighting Quality and Energy Efficiency"; Vienna, Austria. 332-335.

Chirarattananon S., Hien V.D., Chaiwiwatworakul P., Chirarattananon P. 2010. Simulation of transmission of daylight through cylindrical light pipes. Sustainable Energy and Environment, 1; 97-103.

CIE. 2005. Hollow Light Guide Technology and Applications. Technical Report CIE 164:2005. International Commission on Illumination; Austria.

CIE. 2006. Tubular daylight guidance systems. Technical Report CIE 173:2006. International Commission on Illumination; Austria.

Edmonds I. 2010. Transmission of mirror light pipes with triangular, rectangular, rhombic and hexagonal cross section. Solar Energy, 84; 928-938.

Hien, V.D., and Chirarattananon S. 2009. An experimental study of a façade mounted light pipe. Lighting Research and Technology; 41: 123-142.

Kim, J.T., and Kim G. 2010. Overview and new developments in optical daylighting systems for building a healthy environment. Building and Environment; 45: 256-269.

Kocifaj M., Darula S., Kittler R. 2008. HOLIGILM: Hollow light pipe interior illumination method – An analytic calculation approach for cylindrical light-tubes. Solar Energy, 82; 247-259.

Kocifaj M., Kundracik F., Darula S., Kittler R. 2010. Theoretical solution for light transmission of a bended hollow light pipe. Solar Energy, 84 (8); 1422–1432.

Kwok, C.M., and Chung T.M. 2008. Computer simulation study of a horizontal light pipe integrated with laser cut panels in a dense urban environment. Lighting Research and Technology; 40: 287-305.

Laouadi, A., Arsenault, C.D. 2003. Validation of skylight performance assessment software. ASHRAE Transactions, 112, (Pt. 2); 1-13.

Laouadi A., and Coffey B., 2012. The energy performance of the Central Sunlighting System. Journal of Building Performance Simulation, 5(4); 234-247.

Laouadi A., Saber H.H., Galasiu A.D., Arsenault C. 2012a. Tubular daylighting devices - part I: development of an optical model. Submitted to HVAC&R Research Journal.

Laouadi A., Arsenault C., Galasiu A.D., Saber H.H. 2012b. Tubular daylighting devices - part II: validation of the optical model. Submitted to HVAC&R Research Journal.

Laouadi A., Saber H.H., Galasiu A.D., Arsenault C. 2012c. Optical model for prismatic glazing. Submitted to HVAC&R Research Journal.

NRC. 2011. SkyVision v1.2.1 National Research Council of Canada. Available for free download from: http://www.nrc-cnrc.gc.ca/eng/projects/irc/optical-characteristics.html / [Accessed September 2011].

Nutter S.L., Bower C.R., Gebhard M.W., Henz R.M. 1988. The transmittance by a hollow specularly reflecting cylindrical light pipe of isotropically incident radiation. Nuclear Instruments and Methods in Physics Research, A273; 389-396.

Samuhatananon S., Chirarattananon S., Chirarattananon P. 2011. An experimental and analytical study of transmission of daylight through circular light pipes. Leukos, 7(4); 203-219.

Swift P.D., Smith G.B. 1995. Cylindrical mirror lightpipes, Solar Energy Materials and Solar Cells, 36(2); 159-168.

Swift P.D., Smith G.B., Franklin J. 2006. Hotspots in cylindrical mirror lightpipes: description and removal, Lighting Research and Technology, 38(1); 19-31.

Swift P.D., Smith G.B. 2008. Rectangular-section mirror lightpipes, Solar Energy and Solar Materials, 92; 969-975.

Swift P.D. 2010. Splayed mirror lightpipes, Solar Energy, 84;160-165.

Zastrow A., Wittwer V. 1986. Daylighting with mirror lightpipes and with fluorescent planar concentrators, SPIE Materials and Optics for Solar Energy Conversion and Advanced Lighting Technology, 692; 227-234.

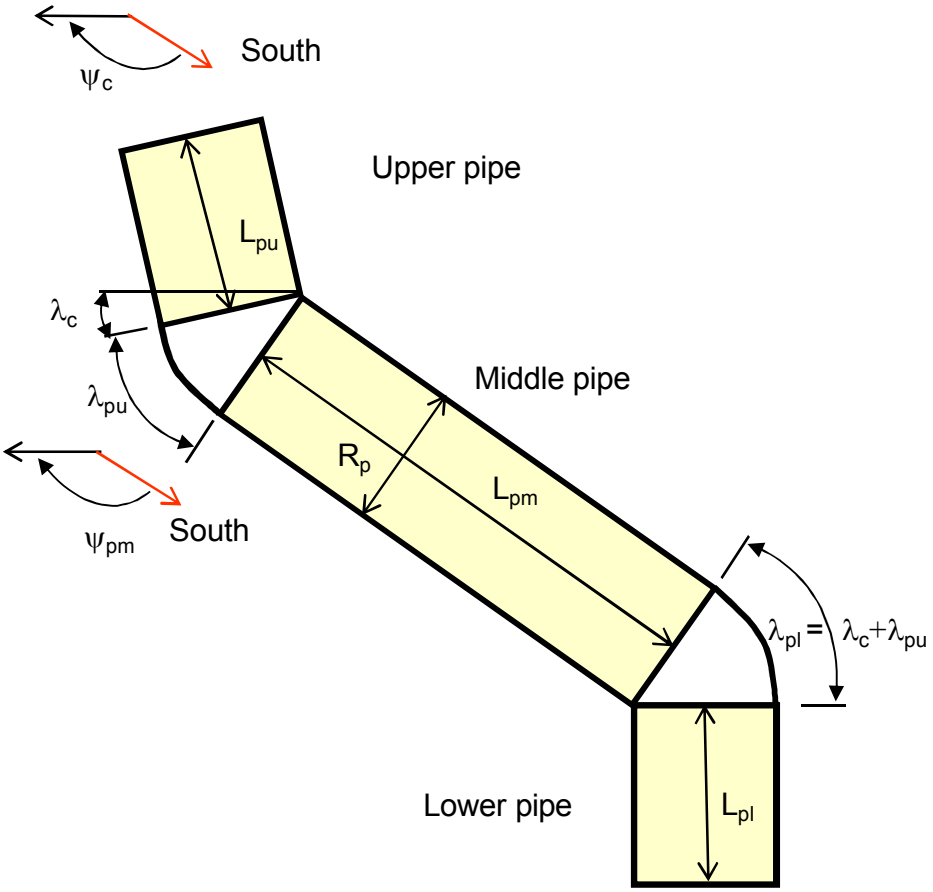


Figure 1. Typical tubular light guide with connection elbows

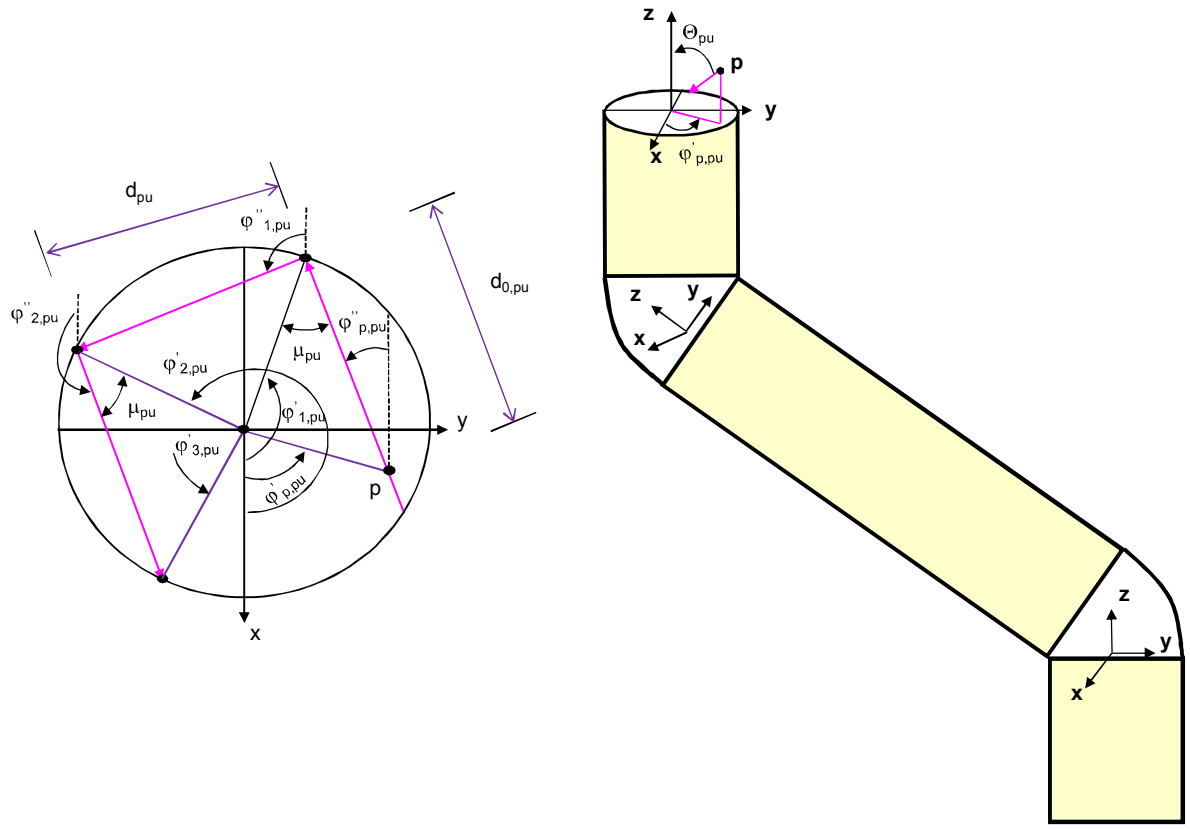


Figure 2. Projected path onto the guide's entrance plane of a conical beam ray transmitting through a bended guide

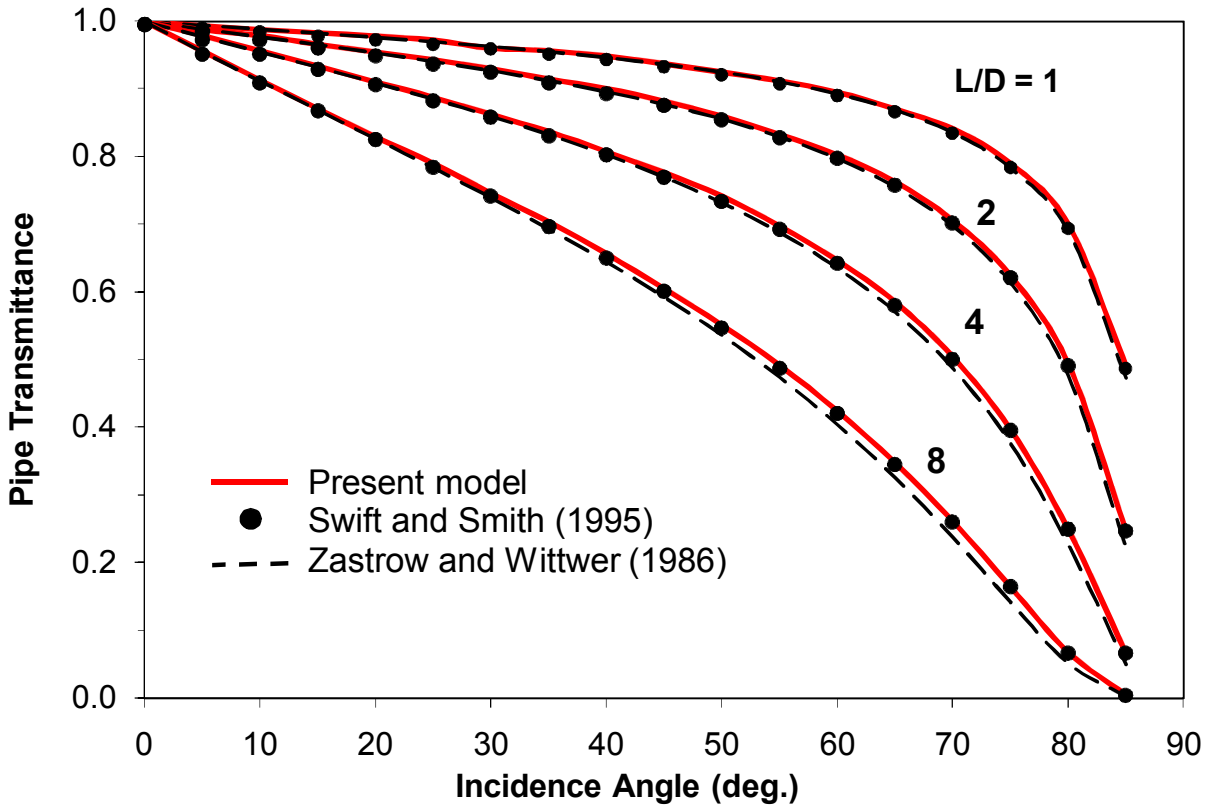


Figure 3 Inter-model comparison for transmittance of a vertical guide

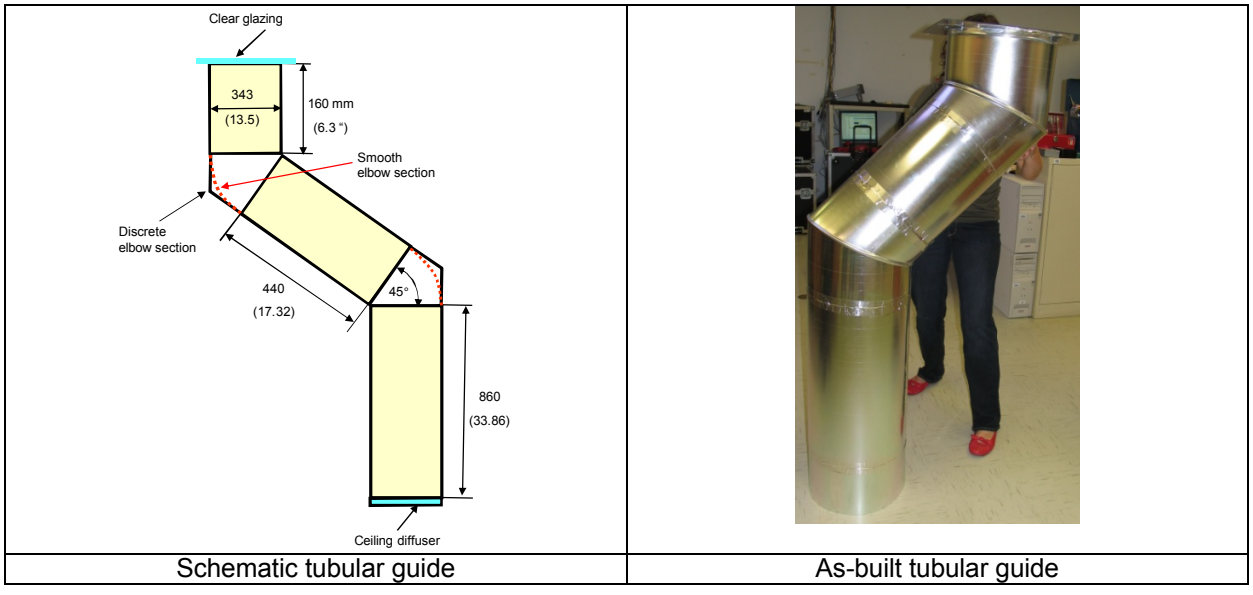


| Schematic tubular guide | As-built tubular guide |
|---|---|

Figure 4 Geometrical details of the custom-made TDD

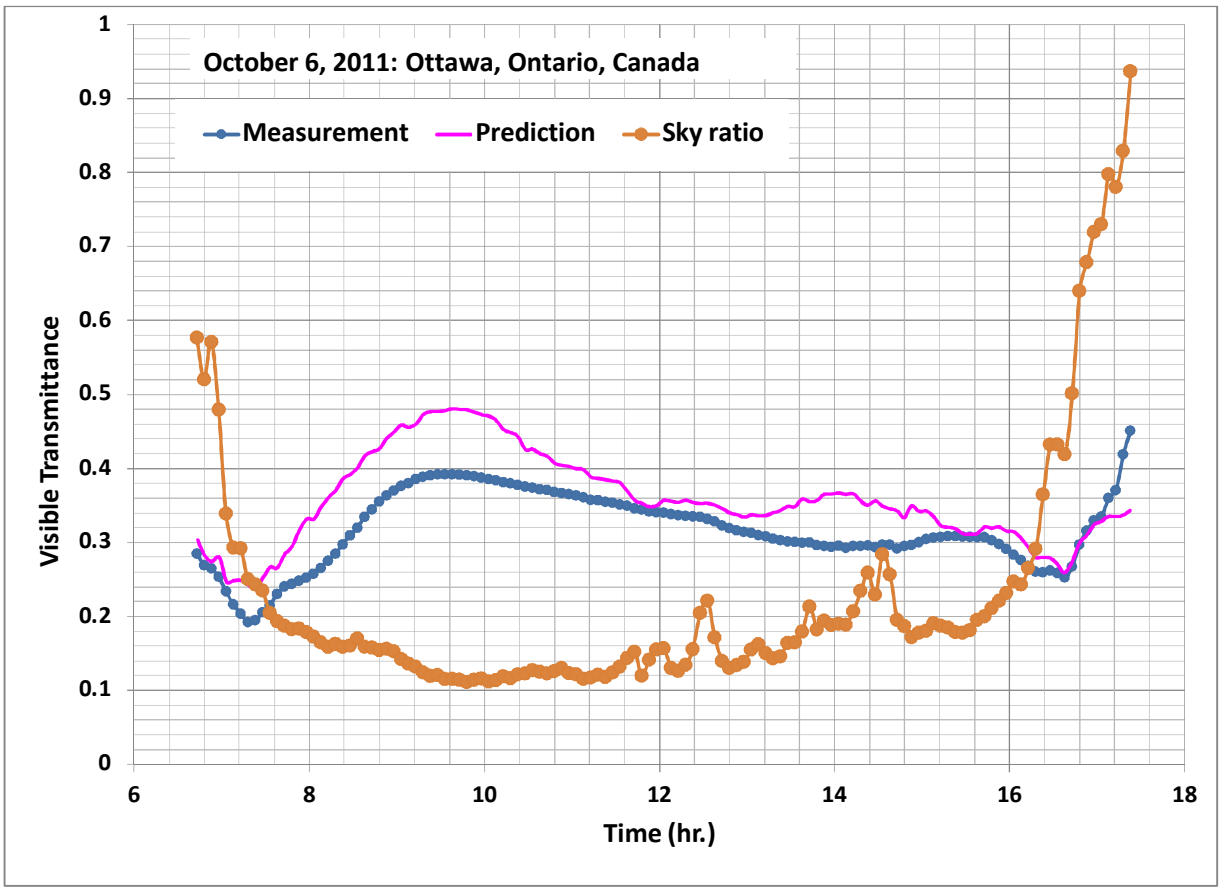


Figure 5 Comparison between the measured and predicted visible transmittance of the custom-made TDD when the middle pipe section was facing the west direction (sky ratio is defined as the diffuse to global horizontal solar irradiances; values < 0.3 indicate clear sky conditions)

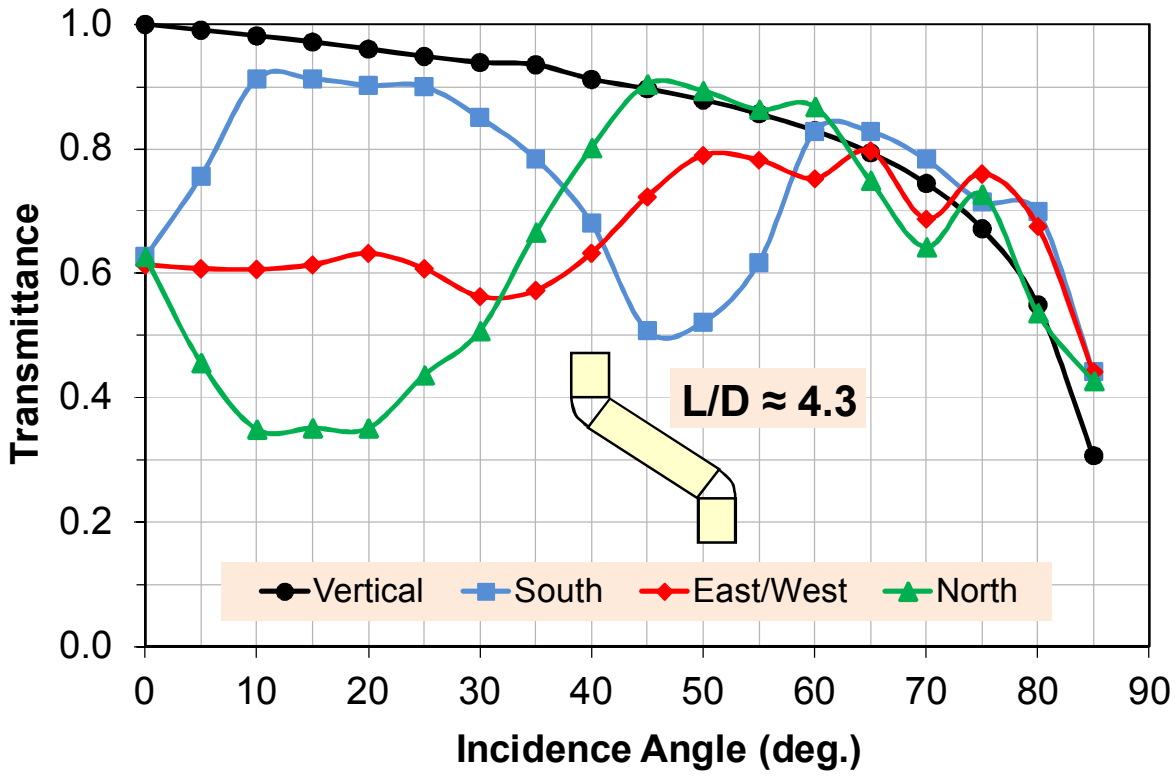


Figure 6 Angular profile of the guide transmittance for various orientations of the middle guide section when the incident sunbeam light is due south.

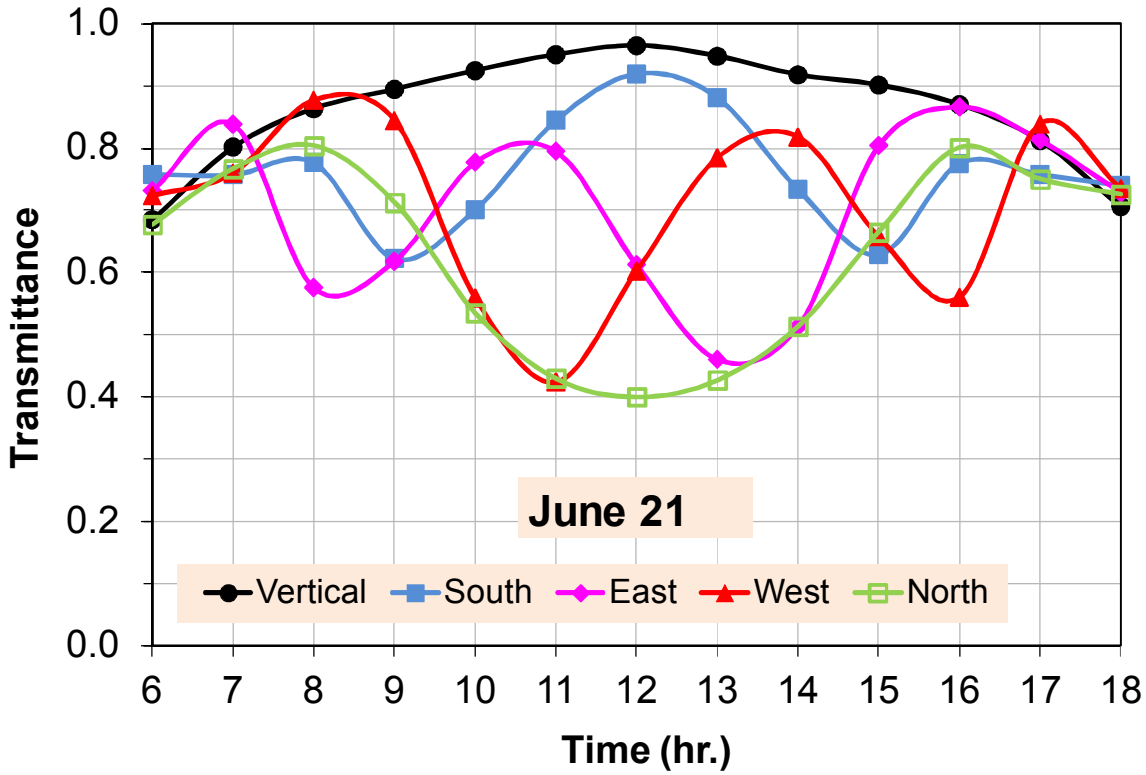


Figure 7 Hourly profile of the guide transmittance for various orientations of the middle guide section on June 21 in Ottawa, Ontario, Canada.

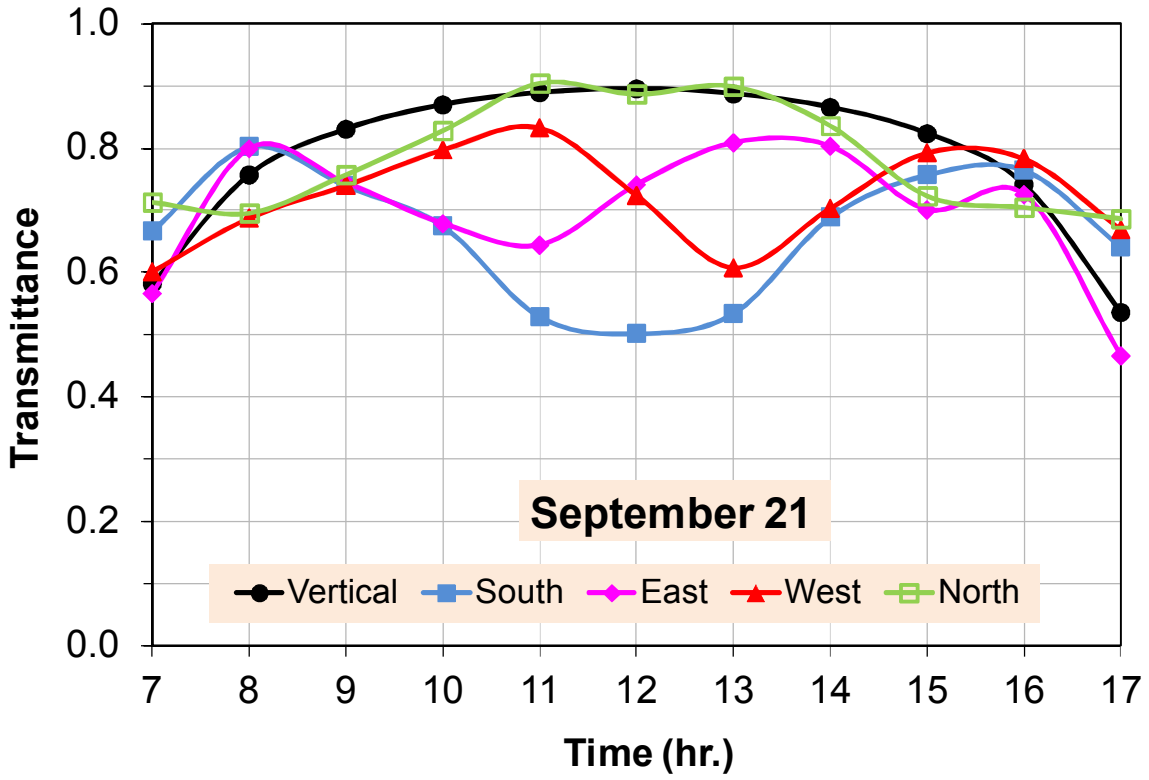


Figure 8 Hourly profile of the guide transmittance for various orientations of the middle guide section on September 21 in Ottawa, Ontario, Canada.

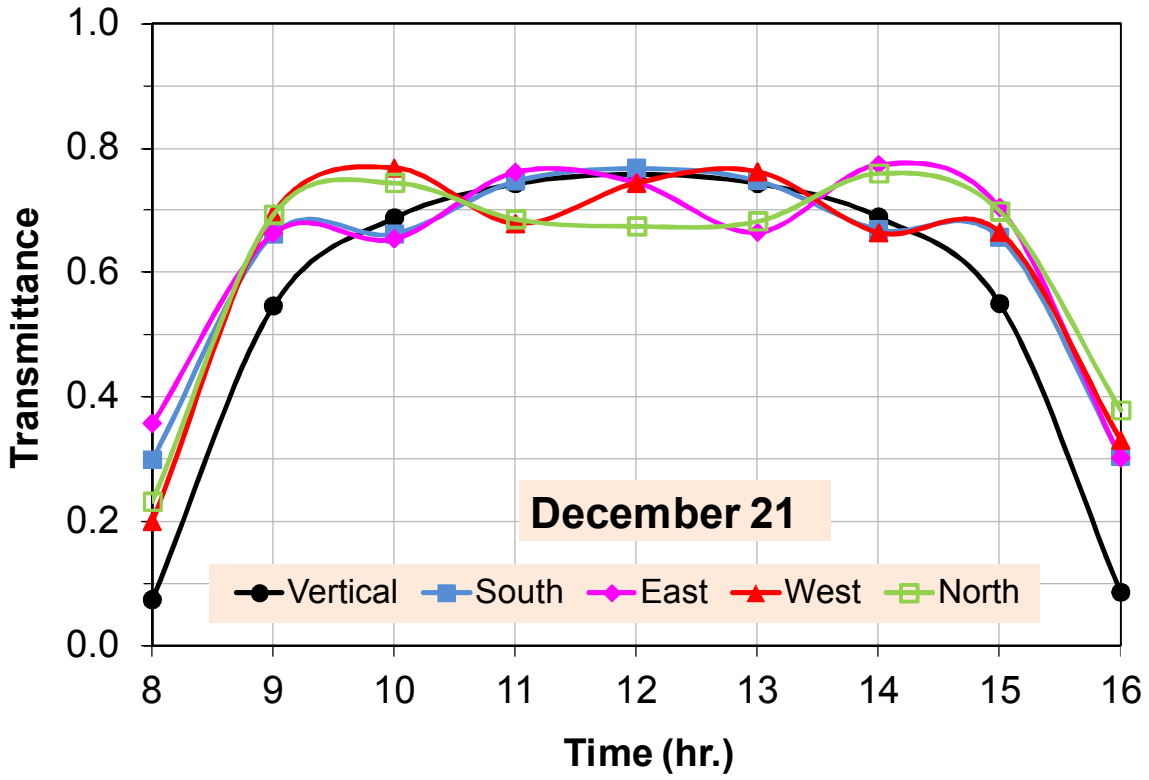


Figure 9 Hourly profile of the guide transmittance for various orientations of the middle guide section on December 21 in Ottawa, Ontario, Canada.

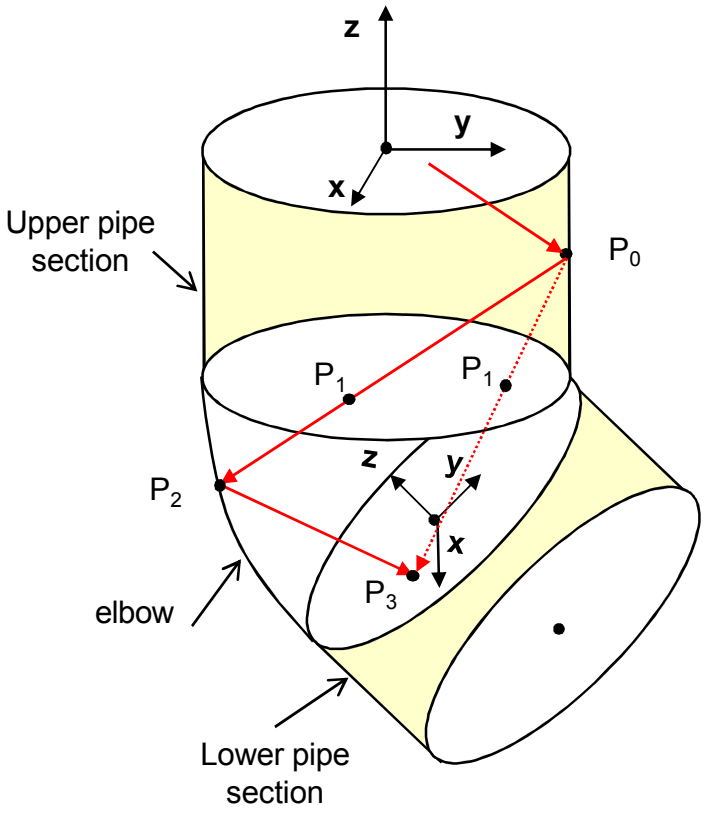


Figure 10. Ray's reflection path at an elbow surface.